Modeling ozone and carbon monoxide redistribution by shallow convection over the Amazonian rain forest

J. Edy, S. Cautenet, P. Brémaud

Modeling ozone and carbon monoxide redistribution by shallow convection over the Amazonian rain forest

J. Edy and S. Cautenet

Laboratoire de Meteorologie Physique, Universite Blaise Pascal, CNRS, Aubiere, France

P. Brémaud

Laboratoire de Physique Atmosphere, Université de l'ile de la Reunion, St. Denis, France

Abstract. During a "locally occurring system" (LOS) in Amazonian forest characterized by an active mixing layer from surface to 1000 m capped by a fossil mixed layer between 1000 and 1500 m, the vertical mixing effects of a shallow cumulus are examined. The explicit redistribution of CO and O_3 has been studied with a two-dimensional convective cloud model coupled with a chemical model including gas and aqueous phases, for a shallow convective situation taken from the GTE/ABLE 2B campaign. The chemistry describes the main oxidation chains of CH_4 and CO in presence of low NO_x concentration in a remote troposphere. Model results compare favorably with observations obtained after development of the shallow convection. The analysis of results explains how a growing and decaying cloud field allows exchanges between a mixing layer, a fossil mixed layer and the free troposphere. An inert tracer study has shown that the layer lying between surface to 500 m is transported up to 2000 m. Even small clouds are responsible for the transport and the transformation of chemical species. Sensitivity tests are performed to evaluate the relative importance of dynamical, microphysical and chemical processes. The cumulus venting is the main process which modifies the trace species redistribution. The O_3 and CO amounts which are transported by a fair-weather cumulus through the boundary layer and free troposphere in the wet season, over a tropical rain forest, are respectively 1.2×10^{23} molecules km^{-2} h^{-1} and 7.7×10^{23} molecules km^{-2} h^{-1}. In tropical regions, over rain forest, even with low NO_x concentration, several cumulus exist every day and the vertical fluxes of some chemical species (like O_3) cannot be neglected.

1. Introduction

The impact of clouds on the transfer of trace species from boundary layer to the free troposphere is very important in both cases of shallow and deep convection. In tropospheric chemistry, three processes are modified by the presence of clouds: the transport of chemical species, the photochemistry and the aqueous phase chemistry. Several authors have demonstrated that convective clouds constitute a mechanism for intense vertical transport, through observations [Ching et al., 1986; Gidel, 1983; Garstang et al., 1988; Lyons et al., 1986] or through inert tracers modeling [Lafore and Moncrieff, 1989; Pickering et al., 1990; Chaumerliac et al., 1989; Renard et al., 1994].

Clouds have not only the potential to transport chemical species from the mixed layer to the overlying free troposphere but also clouds can transform and modify many chemical species by aqueous phase chemistry occurring in droplets [Chameides and Davies, 1982; Jacob, 1986].

In evaluating regional CO and O_3 budgets, Thompson et al. [1994] show the important effect of convective transport over the Central United States. They estimate that both shallow cumulus and synoptic scale weather systems are as efficient as deep convection, but they point out that relative CO and O_3 fluxes due to shallow convection and synoptic scale weather

systems are poorly known. Observations of O_3 distribution inside and outside the clouds apparently lead to different O_3 evolution, depending on the type of clouds (small cumulus or stratiform clouds) [Preiss et al., 1994].

Detailed simulations of clouds and photochemistry in convective situations have highlighted a great degree of variability in dynamical structure and in trace gases redistribution from one event to another one [Scala et al., 1990; Pickering et al., 1990, 1991; Chatfield and Delany, 1990].

All these studies have been achieved using off-line models, without any aqueous chemistry. They show the dominant role of transport during deep convection. More recently, a convection cloud model, explicitly coupled with a gas/aqueous chemical model [Grégoire et al., 1994] exhibits the role of microphysical processes on the redistribution of chemical species among the aqueous and gas phases. With a similar chemistry model, Lelieveld and Crutzen [1991] show the role of clouds on O_3 redistribution. They have estimated that if the air is spending 3 at 4 hours inside the clouds in NO_x poor region, net ozone destruction rates are enhanced by factors ranging from 1.7 to 3.7 [Graedel and Crutzen, 1993].

The preceding works, however, have no experimental support. In this paper, we intend to compare model results with experimental data. Using a cloud model coupled with a gas/aqueous chemical model, we examine the role of the aqueous chemistry in shallow convection when vertical velocity and liquid water content are lower than in deep convection.
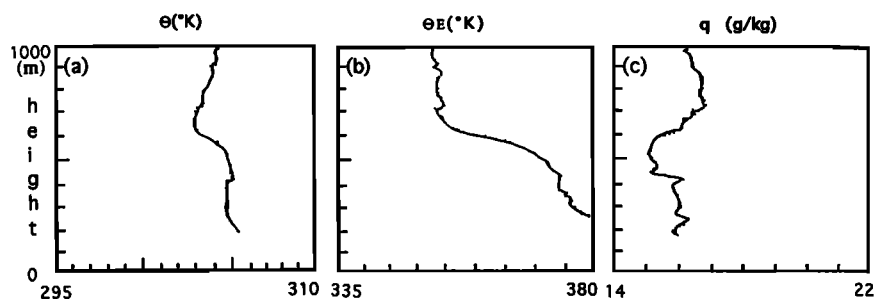
Figure 1. Tethered balloon profile at 1200 local standard time (LST) on May 4, 1987, at Ducke. (a) Potential temperature, (b) equivalent potential temperature, and (c) specific humidity (from M. Garstang, personal communication, 1995).

The equatorial forests are an important source of organic acids [*Talbot et al.*, 1990] which can lead to ozone destruction by aqueous chemistry processes. During the GTE/ABLE2B campaign in 1987 (*Journal of Geophysical Research*, 95, 16,721–17,050, 1990) in Amazonia, an observation of a fair cumulus cloud was performed and vertical profiles of CO and O_3 were measured by an instrumented aircraft, the NASA Electra before and after a succession of convective cells developments. *Ritter et al.* [1990] have examined the influence of such a cloud field on species distributions in the subcloud layer. We use these data to validate our coupled model, and we examine the relative importance of different processes on chemical species distribution due to the presence of small cumulus. Although O_3 is a low soluble species, we want to investigate whether the competition between the three governing processes (transport, photochemistry, aqueous chemistry) is important in a case of shallow convection where the vertical velocities are weak but where the liquid water content is not negligible, as in equatorial forest regions.

After a short presentation of experimental data and of the model, we show the comparison between the simulated and observed profiles. Then, sensitivity tests are performed to assess the relative importance of dynamical, microphysical and chemical processes which are competing inside a shallow cumulus.

The case under study represents a local system which includes a fossil mixed layer lying between 1000 and 1500 m over a tropical rain forest during the wet season. A cumulus penetrates into this layer and destroys it. We examine and evaluate the exchanges between the fossil mixed layer and the mixing layer.

2. Experimental Data

2.1. Meteorological Situation

The synoptic situation for May 4, 1987, over the central Amazon Basin is consistent with fair-weather conditions, associated with shallow convection and small cumulus. This is typically a so-called "locally occurring system" (LOS), characterized by surface divergence until midafternoon, followed by weak convergence associated with the growing convection [*Greco et al.*, 1990].

The description of the meteorological situation is the following: the 700 hPa streamlines pattern shows a convergence line which lies north-south (NS) along 55°W from just north of the equator to about 7.5°S with equatorial vortex centred near 54°W and 0°S. Low level flow (5 m above canopy) at 1120 LST

exhibits divergent easterlies across network. A high-pressure center is observed over Tabatinga; another weak high-pressure center lies on the coast at 10°S, with a ridge between. A NS cloud line is revealed by satellite infrared data at 0900 LST along 55°W with center to the north of Belem coast, whereas a clear area extends to the west of Manaus-Tabatinga. Manaus eastward shows the edge of a system along 55°W. At the 250-hPa level, flow shows an anticyclone centred near 1.5°S, 52.3°W (Amazon mouth) supporting the north/south convergence line. This situation is not likely to undergo rapid changes.

The detailed evolution of the weather from aircraft data is described below:

1. Cloud amounts mainly of fair weather cumulus (CU-1 at 1118 LST) and later (1312 LST) cumulus congestus (CU-2) were present throughout the flight but decreasing in amount from 7/8 sky cover to 4/8 sky cover.

2. Cloud base is ranging between 875 m at 1138 LST and 1100 m at 1501 LST; cloud top locates between 1625 m at 1136 LST and 1719 m at 1501 LST.

3. Inversion base ranging between 1250 m at 1134 LST and 1812 m at 1320 LST.

4. Light showers appeared over the area of operations and were probably present soon after 1300 LST and clearly visible from the aircraft between 1440 and 1457 LST.

On the same day (May 4, 1987), a fair-weather cumulus was studied by *Ritter et al.* [1990] between 1130 LST and 1440 LST. There were no upper level clouds except isolated patches of cirrus far away. By 1130 LST the convective cloud field became more isolated, and cloud cover decreased to 5/8. By 1440 LST the convective cloud development was over.

2.2. Thermodynamical Analyses

This undisturbed day is characterized by a typical mixed layer found above the Amazonian rain forest. The tethered balloon observations and comments which follow have been given by M. Garstang (personal communication, 1995). The tethered balloon observations show a vertical potential temperature profile (Figure 1a) with adiabatic conditions from surface to 1000 m at 1200 LST. Also, the vertical equivalent potential temperature (Figure 1b) and the specific humidity (Figure 1c) profiles look well mixed, although the latter decreases slowly with height over the first 1000 m.

By 1137 LST (Figure 2) a moist adiabatic layer is observed between 1000 and 1200 m, a sharp inversion from 1200 to 1300 m and a secondary moist adiabatic layer from 1300 to 1600 m. The layer from 1000 to 1800 m roughly agrees with the vertical extent of cloud.
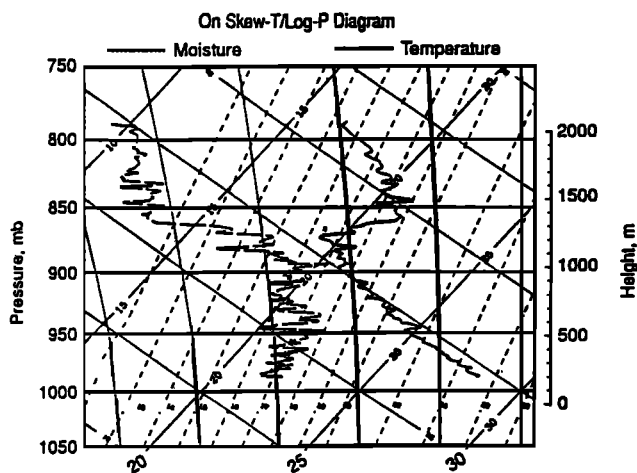
Figure 2. Temperature and moisture profiles obtained during the vertical sounding taken at 1137 LST [from *Ritter et al.*, 1990].

By 1300 LST, gradients are evident in the vertical potential temperature profile (Figure 3a), in the vertical equivalent potential temperature profile (Figure 3b) and in the specific humidity profile (Figure 3c). Downdrafts penetrate the mixing layer and a mixing zone exists between the cloud layer and the mixed layer. This is obviously due to the action of precipitation convection. The depth of the mixed layer has now descended to about 500 m suggesting downward mixing from the cloud layer penetrating to this level.

By 1344 LST we observe (Figure 4) that the inversion zone (from 1400 to 1500 m) has weakened and a moist adiabatic layer extents from 1500 to 1700 m.

2.3. Chemical Data

Figures 5 and 6 represent the CO and O_3 profiles for the two soundings: 1137 and 1344 LST. They both show that O_3 concentration increases with height, while CO concentration decreases. Negative correlation between CO and O_3 in the lower troposphere reflects a sink for O_3 at the surface and a source for CO [*Harris et al.*, 1990]. With low (8 ppt) NO concentration (Table 1) there is no O_3 production; photochemistry represents a weak sink for O_3 [*Jacob and Wofsy*, 1990; *Scala et al.*, 1990].

For O_3 we observe (Figure 5) two mixed layers with constant values: the first below 1000 m where O_3 concentration is 12 ppbv and the second above 1400 m where O_3 concentration is

20 ppbv, which is about twice the values observed near the ground. Between these two mixed layers exists a strong positive gradient of 10 ppbv km^{-1} from 1000 to 1200 m and of 30 ppbv km^{-1} from 1200 to 1400 m associated to the inversion layer. The lower value of 12 ppbv observed below 1000 m is explained by deposition during nighttime and in the morning without exchange with the above layers (as the fossil one for instance).

The CO profile (Figure 5) slowly decreases with height below 1000 m. This profile has a different pattern below 1000 m and above 1000 m, and we observe, as for O_3 profile, that during nighttime and the morning there is no exchange with the above layers. Moreover, above 1000 m a sharp negative CO gradient exists from 1000 to 1200 m with a minimum of 105 ppbv at 1200 m. Then, above 1400 m we see strong alternate positive or negative gradients.

The initial profiles (Figure 5) are consistent with a well established mixed layer (from surface to 800 m) and a shallow cloud convective layer between approximately 900 and 1700 m. Enhanced O_3 content in and above this cloud layer (1000 to above 2000 m) and regions of relatively high CO content (such as the layer near 1500 m) are associated with the previous day's fossil mixed layer and with layer structures due to inversions in the subsidence synoptic scale environment. Frequently, fossil mixed layers over Amazonian rain forest [*Martin et al.*, 1988] are observed, generally during undisturbed days. In this case, the boundary layer at 1137 LST, is characterized by an active
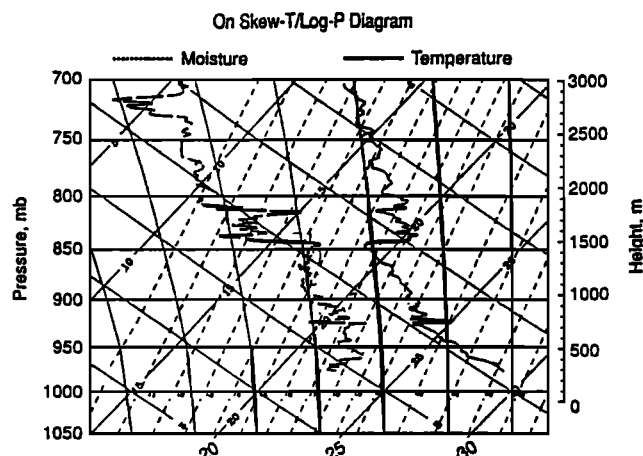

Figure 4. Temperature and moisture profiles obtained during the vertical sounding taken at 1344 LST [from *Ritter et al.*, 1990].
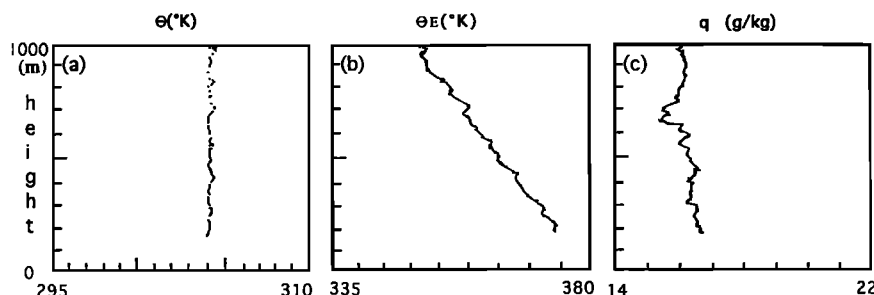

Figure 3. Tethered balloon profile at 1300 LST on May 4, 1987, at Ducke. (a) Potential temperature, (b) equivalent potential temperature, and (c) specific humidity (from M. Garstang, personal communication, 1995).
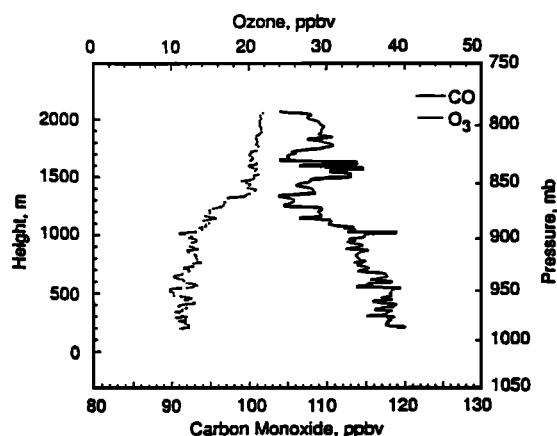
Figure 5. O_3 (dashed line) and CO (solid line) species mixing ratio profiles obtained during the initial sounding of Figure 1 [from *Ritter et al.*, 1990].

mixing layer from surface to 1000 m capped by a fossil mixed layer between 1000 and 1500 m, mixed but not mixing.

In Figure 6, after the development of shallow convection, we observe a smoothing in the O_3 vertical profile and the gradients are much more homogeneous than in Figure 5. The CO profile (Figure 6) is less mixed than O_3 and has a similar shape than the water vapor profile. This pattern may be explained because the CO source is the ground surface. Figure 6 profiles exhibit the clear signature of a precipitating cumulus which mixes both layers (fossil and underlying mixing layer).

In the case of O_3, higher cloud layer values of O_3 have been mixed downward into the mixed layer and lower mixed layer values elevated into the cloud layer. In the case of CO, high values prevail near surface (below 750 m), but a general decrease with cloud/precipitation mixing has occurred above 750 m. The stratified and layered nature is evident.

3. Description of the Chemical Transport Cloud Model

The chemical model [*Grégoire et al.*, 1994] is coupled with a convection model. It monitors 12 chemical species in gaseous and aqueous phases as introduced by *Lelieveld and Crutzen* [1990,
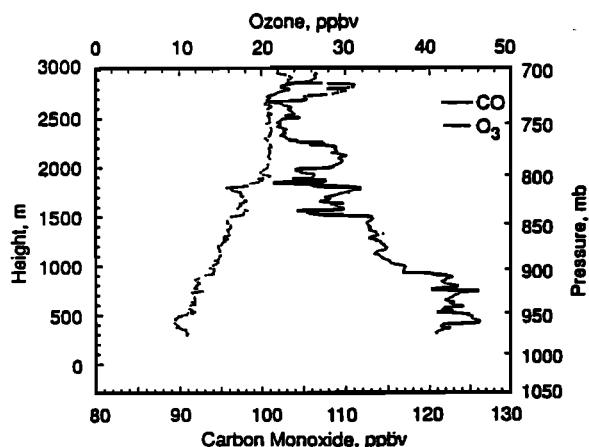

Figure 6. O_3 (dashed line) and CO (solid line) species mixing ratio profiles obtained during the sounding of Figure 4 [from *Ritter et al.*, 1990].

1991]. It describes the main oxidation chains of CH_4 and CO in presence of NO_x in a remote troposphere. Its kinetic scheme presented in Table 2 contains 26 reactions and equilibrium in the gas phase, 16 gas/aqueous phase equilibrium, and 11 aqueous phase reactions. The rate of reaction G4 has been modified, following *Stockwell* [1994], to account for its dependency on water vapor and temperature, a feature which was neglected by *Lelieveld and Crutzen* [1991] and also by *Grégoire et al.* [1994]. The photolysis rates calculated according to *Madronich* [1987] for local conditions are assumed constant with time, but may vary with the altitude and the location of the cloud layers. The complete chemical scheme then leads to a set of two primary equations which express the rate of concentration changes between gas and aqueous phases, including mass transfer considerations. Those equations are solved by the *Hesstvedt* [1978] solver with a time step of 0.5 s when cloud is present, and a time step of 15 s otherwise. For more details, the reader is referred to *Grégoire et al.* [1994].

The cloud model is a two-dimensional (x, z), time-dependent, Eulerian scheme [*Cautenet and Lefeivre*, 1994]. It is nonhydrostatic and anelastic. Three bulk water categories are considered here: vapor, cloud water and rain water. These hydrometeors interact through a variety of physical processes (e.g., condensation, evaporation, autoconversion, coalescence, accretion, and collection). The basic assumptions in the microphysical processes used are (1) a monodisperse, time invariant cloud droplet population in which the total number of droplets is fixed; (2) droplet coalescence (autoconversion) computed using the *Kessler* [1969] formulation with a threshold; and (3) rain distribution following *Marshall and Palmer*'s [1948] distribution. Surface energy fluxes are prescribed which allow triggering and maintenance of cloud cycles. The horizontal spatial grid resolution is 200 m. The vertical spatial grid resolution is 100 m in order to be able to describe a fine structure of thermodynamic profile commonly observed within shallow cloud layers. The overall dimension of the modeled domain is 3.2 km in the vertical and 6.4 km in the horizontal. The time step of integration is 15 s. The duration of the simulation is 2 hours.

We initialize the model with the atmospheric sounding (Figure 2) along with O_3 and CO profiles (Figure 5) at 1137 LST. For the other species, we take vertically homogeneous profiles in ppb (Table 1), according to *Jacob and Wofsy* [1990] and *Singh et al.* [1990]. The pH is held constant and equal to 5, a typical value of precipitation acidity during ABLE 2B campaign [*Jacob and Wofsy*, 1990].

The ground budget is prescribed as follows [*Fitzjarrald et al.*, 1990]: the net radiative flux at the beginning of the simulation

Table 1. Initial Values of Chemical Species in the Gas Phase That Are Used to Initialize the Chemical Module

Chemical Species	Concentrations
O3	from the sounding
H2O2	2.5 parts per billion (ppb)
CH3OOH	2.0 ppb
CH2O	0.5 ppb
CO	from the sounding
HNO3	0.2 ppb
HO2	8.8 parts per trillion (ppt)
OH	0.08 ppt
NO2	12.0 ppt
NO	8.0 ppt
CH3OO	4.95 ppt
HCOOH	0.3 ppb

Table 2. List of Reactions With Their Corresponding Rate Constants for Gas Phase, Gas-Aqueos Phase and Aqueous Equilibria, and Aqueous Phase

	Scheme	Rate Constants
	Gas Phase Reaction	
G1	$O_3 + H_2O + h\nu \rightarrow 2OH \cdot + O_2$	calculated from *Madronich* [1987]
G2	$O_3 + OH \cdot \rightarrow HO_2 \cdot + O_2$	$1.6 \times 10^{-12} \exp(-940/T)$
G3	$O_3 + HO_2 \cdot \rightarrow OH \cdot + 2O_2$	$1.1 \times 10^{-14} \exp(-500/T)$
G4	$2HO_2 \cdot \rightarrow H_2O_2 + O_2$	$(2.3 \times 10^{-13} \exp(600/T) + 1.7 \times 10^{-33} [M] \exp(1000/T)) [1 + (1.4 \times 10^{-21}) [H_2O] \exp(2200/T)]$
G5	$H_2O_2 + h\nu \rightarrow 2OH \cdot$	calculated from *Madronich* [1987]
G6	$H_2O_2 + OH \cdot \rightarrow HO_2 \cdot + H_2O$	$3.3 \times 10^{-12} \exp(-200/T)$
G7	$CH_4 + OH \cdot + O_2 + M \rightarrow CH_3O_2 \cdot + H_2O + M$	$2.3 \times 10^{-12} \exp(-1700/T)$
G8	$CH_3O_2 \cdot + HO_2 \cdot \rightarrow CH_3O_2H + O_2$	4.0×10^{-12}
G9	$CH_3O_2H + O_2 + h\nu \rightarrow CH_2O + HO_2 \cdot + OH \cdot$	calculated from *Madronich* [1987]
G10	$CH_3O_2H + OH \cdot \rightarrow CH_3O_2 \cdot + H_2O$	5.6×10^{-12}
G11	$CH_3O_2H + OH \cdot \rightarrow CH_2O + OH \cdot + H_2O$	4.4×10^{-12}
G12	$CH_2O + 2O_2 + h\nu \rightarrow CO + 2HO_2$	calculated from *Madronich* [1987]
G13	$CH_2O + h\nu \rightarrow CO + H_2$	calculated from *Madronich* [1987]
G14	$CH_2O + OH \cdot + O_2 \rightarrow CO + HO_2 \cdot + H_2O$	1.1×10^{-11}
G15	$CO + OH \cdot + O_2 + M \rightarrow CO_2 + HO_2 \cdot + M$	2.4×10^{-13}
G16	$NO + O_3 \rightarrow NO_2 + O_2$	$2.0 \times 10^{-12} \exp(-1400/T)$
G17	$NO_2 + O_2 + h\nu \rightarrow NO + O_3$	calculated from *Madronich* [1987]
G18	$NO + HO_2 \cdot \rightarrow NO_2 + OH \cdot$	$3.7 \times 10^{-12} \exp(240/T)$
G19	$NO + CH_3O_2 \cdot + O_2 \rightarrow NO_2 + CH_2O + HO_2 \cdot$	$4.2 \times 10^{-12} \exp(180/T)$
G20	$NO_2 + OH \cdot + M \rightarrow HNO_3 + M$	1.2×10^{-11}
G21	$HNO_3 + h\nu \rightarrow NO_2 + OH$	calculated from *Madronich* [1987]
G22	$CH_2O + HO_2 \cdot \leftrightarrow \cdot O_2CH_2OH$	6.7×10^{-15}
G23	$\cdot O_2CH_2OH + HO_2 \cdot \rightarrow HCO_2H + H_2 \cdot O + O_2$	2.0×10^{-12}
G24	$\cdot O_2CH_2OH + NO + O_2 \rightarrow HCO_2H + HO_2 \cdot + NO_2$	7.0×10^{-12}
G25	$2 \cdot O_2CH_2OH + O_2 \rightarrow 2HCO_2H + 2HO_2 \cdot$	1.2×10^{-13}
G26	$HCO_2H + OH \cdot + O_2 \rightarrow CO_2 + HO_2 \cdot + H_2O$	3.2×10^{-13}
	*Gas-Aqueous and Aqueous Phase Equilibria**	
E1	$H_2O \leftrightarrow H^+ + OH^-$	$1.0 \times 10^{-14} \exp[-6716(1/T - 1/298)]$
H1	$O_{3(g)} \leftrightarrow O_{3(aq)}$	$1.1 \times 10^{-2} \exp[2300(1/T - 1/298)]$
H2	$H_2O_{2(g)} \leftrightarrow H_2O_{2(aq)}$	$7.4 \times 10^4 \exp[6615(1/T - 1/298)]$
E2	$H_2O_{2(aq)} \leftrightarrow HO_2^- + H^+$	$2.2 \times 10^{-12} \exp[-3730(1/T - 1/298)]$
H3	$CH_3O_2H_{(g)} \leftrightarrow CH_3O_2H_{(aq)}$	$2.2 \times 10^2 \exp[5653(1/T - 1/298)]$
H4	$CH_2O_{(g)} \leftrightarrow CH_2(OH)_{2(aq)}$	$2.0 \times 10^{-12} \exp[6425(1/T - 1/298)]$
H5	$HNO_{3(g)} \leftrightarrow HNO_{3(aq)}$	$5.6 \times 10^{-3} \exp[8700(1/T - 1/298)]$
E3	$HNO_{3(aq)} \leftrightarrow H^+ + NO_3^-$	15.4
H6	$HO_2 \cdot _{(g)} \leftrightarrow HO_2 \cdot _{(aq)}$	$2.0 \times 10^3 \exp[6600(1/T - 1/298)]$
E4	$HO_2 \cdot _{(aq)} \leftrightarrow H^+ + O_{2(aq)}^-$	3.5×10^{-5}
H7	$OH \cdot _{(g)} \leftrightarrow OH \cdot _{(aq)}$	9.0×10^3
H8	$NO_{2(g)} \leftrightarrow NO_{2(aq)}$	$6.4 \times 10^{-3} \exp[2500(1/T - 1/298)]$
H9	$NO_{(g)} \leftrightarrow NO_{(aq)}$	$1.9 \times 10^{-3} \exp[1480(1/T - 1/298)]$
H10	$CH_3O_2 \cdot _{(g)} \leftrightarrow CH_3O_2 \cdot _{(aq)}$	$2.0 \times 10^3 \exp[6600(1/T - 1/298)]$
H11	$HCO_2H_{(g)} \leftrightarrow HCO_2H_{(aq)}$	$3.7 \times 10^3 \exp[5700(1/T - 1/298)]$
E5	$HCO_2H_{(aq)} \leftrightarrow H^+ + HCO_2^-$	$1.8 \times 10^{-4} \exp[-1510(1/T - 1/298)]$
	Aqueous Phase Reaction	
A1	$H_2O_2 + h\nu \rightarrow 2OH \cdot$	$G5 \times 1.6$
A2	$O_3 + h\nu \rightarrow H_2O_2 + O_2$	$G1 \times 1.6$
A3	$CH_2(OH)_2 + OH \cdot + O_2 \rightarrow HCO_2H + HO_2 \cdot + H_2O$	$2.0 \times 10^9 \exp[-1500(1/T - 1/298)]$
A4	$HCO_2H + OH \cdot + O_2 \rightarrow CO_2 + HO_2 \cdot + H_2O$	$1.6 \times 10^8 \exp[-1500(1/T - 1/298)]$
A5	$HCO_2^- + OH \cdot + O_2 \rightarrow CO_2 + HO_2 \cdot + OH^-$	$2.5 \times 10^9 \exp[-1500(1/T - 1/298)]$
A6	$O_3 + O_2^- + H_2O \rightarrow OH \cdot + OH^- + 2O_2$	$1.5 \times 10^9 \exp[-1500(1/T - 1/298)]$
A7	$HO_2 \cdot + O_2^- + H_2O \rightarrow H_2O_2 + OH^- + O_2$	$1.5 \times 10^9 \exp[-1500(1/T - 1/298)]$
A8	$H_2O_2 + OH \cdot \rightarrow HO_2 \cdot + H_2O$	$1.0 \times 10^8 \exp[-1715(1/T - 1/298)]$
A9	$CH_3O_2 \cdot + O_2^- + H_2O \rightarrow CH_3O_2H + OH^- + O_2$	$5.0 \times 10^7 \exp[-1610(1/T - 1/298)]$
A10	$CH_3O_2H + OH \cdot \rightarrow CH_3O_2 \cdot + H_2O$	$2.7 \times 10^7 \exp[-1715(1/T - 1/298)]$
A11	$CH_3O_2H + OH \cdot \rightarrow CH_2(OH)_2 + OH \cdot$	$1.9 \times 10^7 \exp[-1860(1/T - 1/298)]$

*Rate constants K_{298}.

(on May 4, 1987 at 12 hours) is 450 W m^{-2} and slowly diminishes during the simulation owing to cloud development and decreasing incident radiative solar flux. The sensible heat flux is 100 W m^{-2} and the latent heat flux is 350 W m^{-2} to account for the strong precipitation which had taken place on the previous day, therefore involving a strong evapotranspiration.

The aim of the modeling study is to test the ability of the model to retrieve the observed data (Figures 3 and 4) at 1344 LT. We want to examine and evaluate the exchanges between the lower layer and free troposphere via the mixing and the fossil layers.

4. Results and Discussion

4.1. Meteorological Results

The cloud field simulated during 2 hours, on May 4, 1987, is characterized by different cells. The domain is small (6.4 km),

but the unique cloud, which undergoes various life cycles, is thought to represent a much longer distribution. During the simulation the cloud cell periodically grows and decays over a period of about 140 min, with a top ranging between 1000 and 2000 m (Figure 7g). Figure 8 displays the growing and decaying cells (shown by the vertical velocity and liquid content evolution's) with about a 10 to 20-min period.

At the center of the cell convection, the cloud liquid water content has maximum values of about 1.5 g kg^{-1} and maximum vertical velocity of about 4 m s^{-1} (Figure 8).

At the start of the cloud development a strong convective movement is organized. After 30 min the field of vertical motion extends from surface to 2000 m (Figures 7a and 7b). Horizontally, the cell disturbs a large zone. The active mixing layer is mixed with the fossil layer. During the maximum development, exchanges exist from surface to cloud top, that is, about the free troposphere. When the cloud cell decreases, the convection zone is located below 1500 m and extends horizontally over 3 km. The downdrafts are more intense than updrafts (Figures 7c and 7d). At the end of our simulation the cloud convection is weak, and light showers are observed. A separated evolution between the cloud convection itself and the mixing layer is observed, in the horizontal and vertical wind fields after about 120 min (Figures 7e, 7f, and 7g). There are two convective cells: the first from the ground to 1000 m and the second from 1300 to 2200 m where is found a cloud cell.

The observed thermodynamic structure (Figure 4) exhibits a dry adiabatic layer from 400 to 700 m, a thick inversion layer from 1400 to 1600 m and a moist adiabatic layer from 1600 to 1800 m which explains the two modeled cells. A cloud cell is connected to the moist adiabatic layer, and a dry convective cell is the counterpart of the dry adiabatic layer. The upper part of cloud allows the venting through free troposphere, since the low part evaporates in boundary layer. The stability is restored in the boundary layer and when the cloud is less supplied by upward water vapor vanishes very quickly. The cloud evaporates and precipitates weak showers and we observe that convection cell is separated in two parts (Figures 7e and 7f).

4.2. Species Behavior in the Cloud Center

Within the cloud, at 1500-m level, at the center of the convective cell, are displayed (Figures 8 and 9) the cloud liquid water content (grams per kilogram), the vertical speed (meters per second), the O_3 and CO concentration normalized by the initial values during 140 min. The liquid water content maximum is associated with vertical speed maximum. The increase in liquid water content is connected to enhanced latent heat release which in turn induces large positive vertical speeds. Conversely, negative vertical velocities are driven by the evaporative decay of liquid water content. In fact, as mentioned above, several cloud cells cycles are described. CO and O_3 concentrations are evolving out of phase e.g. when an increase in CO concentration is observed, a decrease in O_3 concentration occurs in the same time, and conversely. The main source of CO is at the ground surface and CO concentration decreases with altitude, while O_3 is generated by photochemistry within the boundary layer so that O_3 concentration increases with altitude.

4.3. Comparison Between Modeled and Observed Profiles

Figure 10 displays a comparison between modeled and measured profiles at the end of cloud convection. There is a standard deviation of about 10% between the modeled and measured profiles for both CO and O_3. The modeled profiles are more smoothed than experimental ones. In our model we have taken into account the dynamical, microphysical, gas and aqueous chemistry processes but not the uptake by the forest canopy.

During the shallow convection, cumulus cell can mix both layers (fossil and underlying mixing layer) so that the fossil mixed layer is destroyed. For O_3 the profile is simply linearized within the cloud as well as below the cloud. The in-cloud smoothing is obviously driven by the vertical speeds which are very high in this zone. For CO the source is supplied by the rain forest canopy, and its profile is linearized only within the cloud.

When the convection vanishes, in this subcloud layer, two weak cells of convection, in-cloud (moist) and subcloud (dry), are modeled and can explain the different behaviors of CO and O_3 near surface. The strength of dynamical processes decays near the ground surface. The lower cell below 1000 m is capped by an inversion layer. This features explain the CO accumulation at 800 m, obvious in the profile (Figure 10).

4.4. Inert Tracer Study

A layered tracer scheme is used to investigate the transport efficiency of a shallow convection cloud field. At initial time an inert tracer layer is introduced into the model domain between surface and 500 m. At the end of simulation (140 min) we see (Figure 11) that the inert tracer has propagated up to 2000 m. Forty percent of the initial concentration reaches 2.0 km in altitude over 2 km wide for a 6.4-km simulated domain in the horizontal. The compounds lying near surface can be transported above boundary layer, in the free troposphere by a fair-weather cumulus. Several studies have been performed for deep and organized cloud convection, in particular squall lines in Amazonia. A squall line is divided into two components: convective and stratiform. These two regions contribute to vertical transport [Houze, 1989]. Thirty to fifty percent of the vertical transport is accomplished by the hot towers (convective region), and the remainder is brought about the trailing stratiform region which also participates to transport in the upper troposphere by anvil region [Greco et al., 1994]. Simulated results (tracer 2 [Scala et al., 1990]) for a squall line show that 40% of initial concentration reaches 3.5 km over 10 km wide and only 2.0 km in altitude over 30 km wide for 160 km simulated domain. Therefore, in a squall line, although vertical transport can be observed up to the upper troposphere, a large amount of surface tracer reaches only 2000 m. The squall lines cover large areas, but these meteorological events have a rare occurrence on the overall year. If we examine the lower troposphere where the biogenical emissions take place, the shallow convection plays a role which must be taken into account. It is quite realistic to hypothesize that, even though fair-weather cumulus induces weaker vertical fluxes than squall lines, they are more frequent and can contribute to nonnegligible amounts of net vertical transport of some surface trace compounds in lower troposphere (from surface to 2000 m).

4.5. Main Processes Driving the Chemical In-cloud Species Redistribution

Sensitivity tests have been performed to evaluate the relative importance of different processes (transport, photochemistry or aqueous chemistry) on chemical species distribution due to the presence of small cumulus.

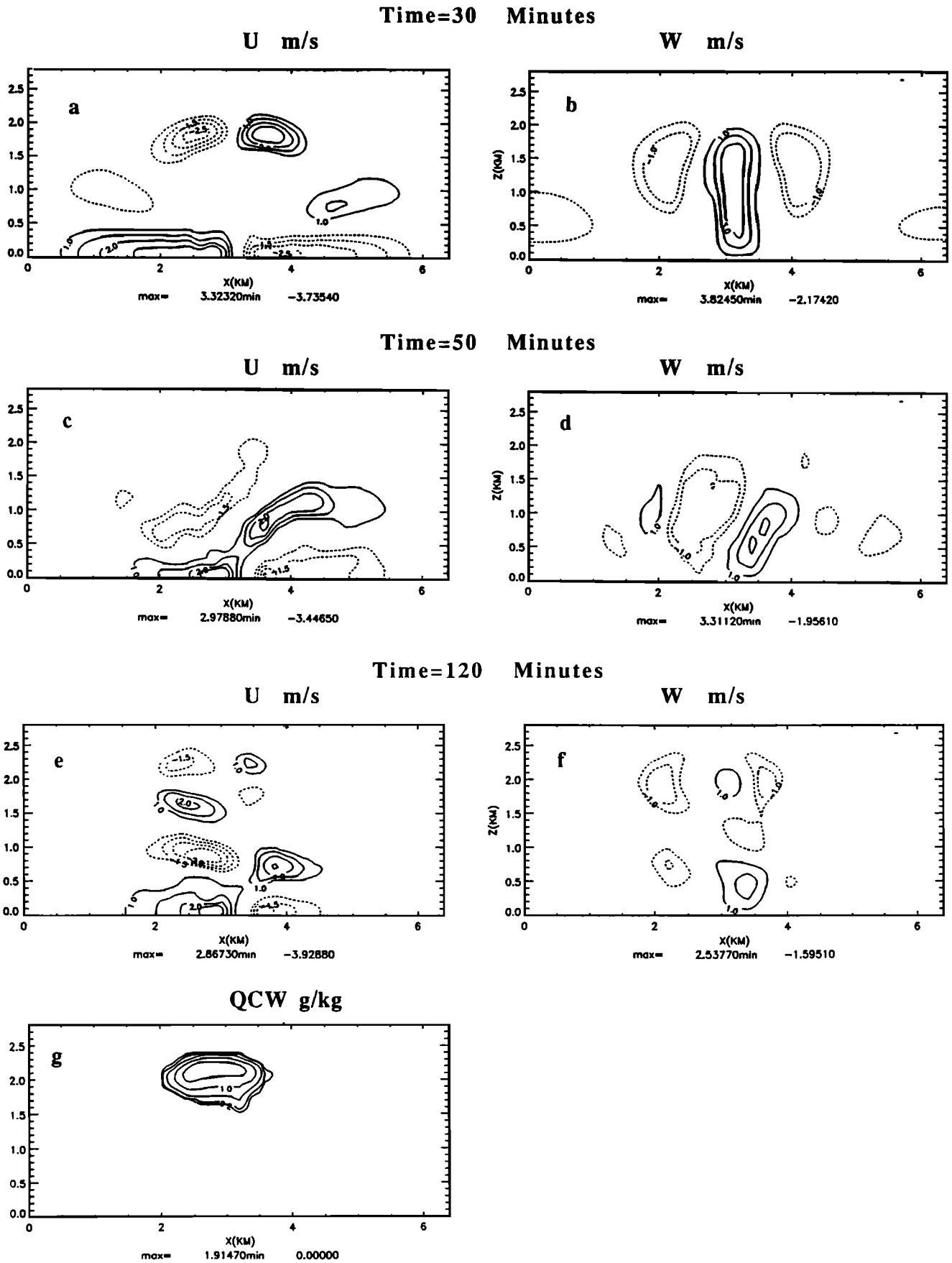The evolution of CO and O_3 concentration normalized by

Time=30   Minutes

U   m/s

W   m/s

Time=50   Minutes

U   m/s

W   m/s

Time=120   Minutes

U   m/s

W   m/s

QCW   g/kg

Figure 7.   Isolines of horizontal wind, U in meters per second, vertical wind, W in meters per second and cloud liquid water content, QCW in grams per kilogram at different times of the simulation.
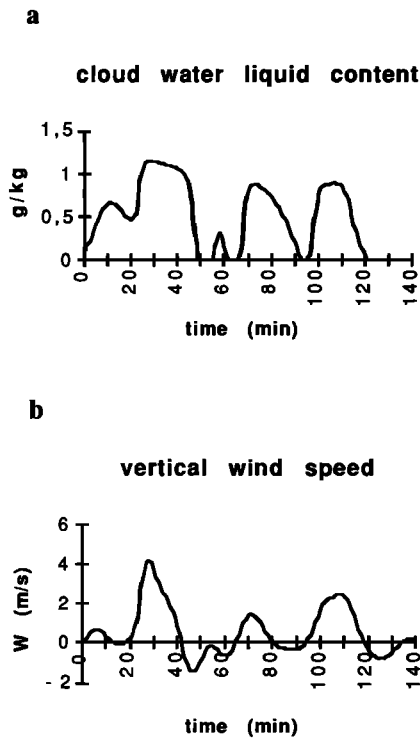
Figure 8. At 1500 m in center of convection, time evolution during 140 min, of cloud liquid water content (grams per kilogram), of vertical speed (meters per second).

initial value in center of cloud are examined (Figure 12). Curve 1 describes the complete scheme which takes into account all the processes: dynamical, microphysical, and chemical. If the aqueous chemical reactions and the transfer between aqueous and gaseous phases are neglected, the CO concentration is not modified, because it is not soluble, so that curve 2 is not different from curve 1. For O_3 there is a very low increase associated with low O_3 solubility and O_3 destruction by aqueous chemistry process. These effects remain unimportant. We notice that the increase in O_3 follows the liquid water content maximum (condensation), while the decrease of O_3 follows the liquid water content minima (evaporation). For curve 3, we also neglect the dynamical processes, only the gaseous chemical reactions are taken into account like in a box model. In this case, the CO and O_3 concentrations do not vary.
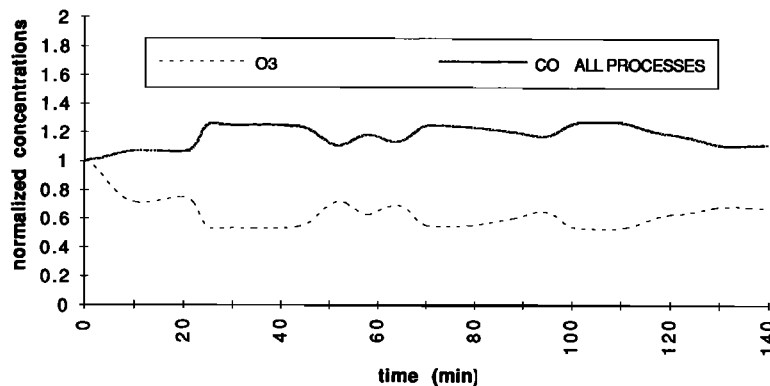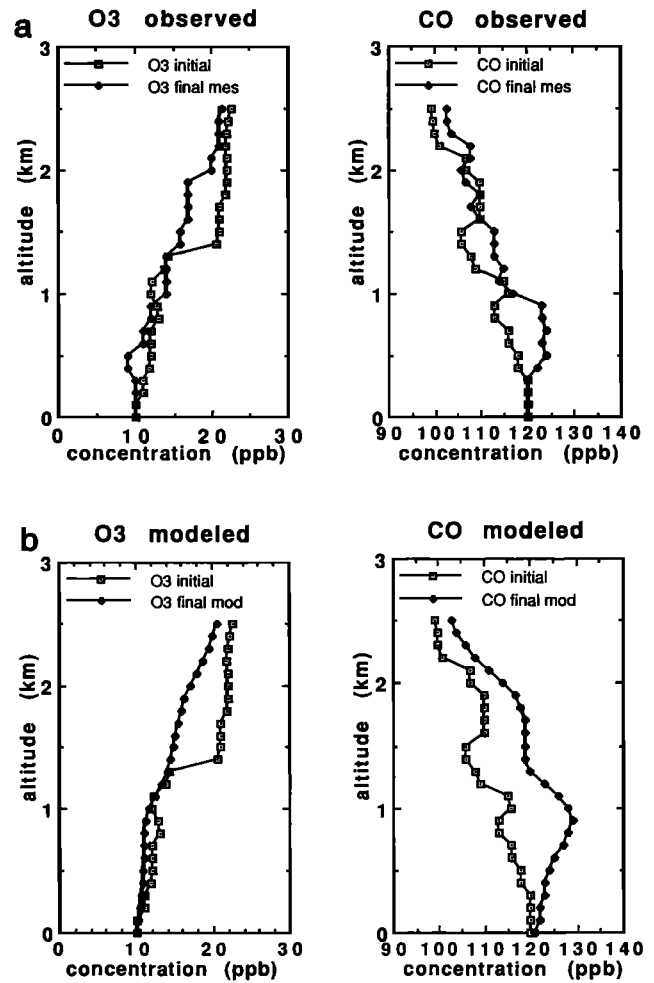

Figure 10. O_3 and CO species mixing ratio profiles (a) obtained during the experiment before and after the presence of cloud and (b) obtained by the simulation after the presence of cloud.

For this kind of cloud (fair-weather cumulus), with low values in NO and O_3 concentration, CO and O_3 behave like inert gases. Photochemistry represents a very low sink for O_3 [Scala et al., 1990]. This phenomenon can be explained as follows: first, CO gas reacts very little with other gases which are in the

Figure 9. At 1500 m in center of convection, time evolution during 140 min, of O_3 and CO concentration normalized to initial value.
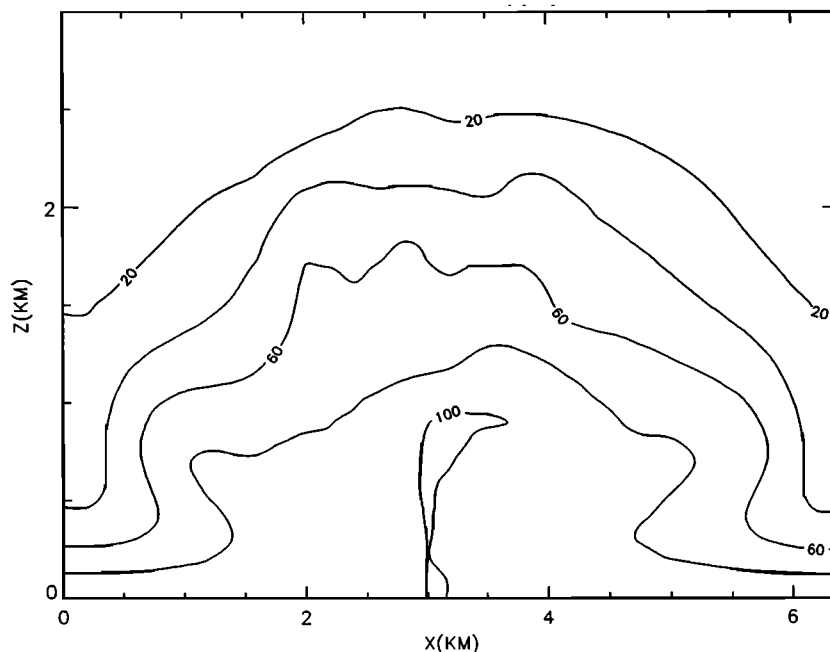
Figure 11. The simulated modification of an inert tracer by cloud transport after 140 min. The initial distribution lies between surface and 500 m.

atmosphere, and moreover, CO concentration is ten times greater than other gases, including O_3. The evolution of CO and O_3 concentration profiles are out of phase: CO increases with height, while O_3 decreases. The vertical cloud transport is the main process driving chemical species redistribution. We see that even fair-weather cumulus perform transport or transformation.

5. Evaluation of Cumulus Venting Over a Tropical Rain Forest During the Wet Season

A survey of shallow (fair-weather) cumulus clouds over part of Amazonia yields to evidence of enhanced frequency of occurrence of clouds over zone (in particular along the highway) where the forest had been cleared during the 1988 dry season

[*Cutrim et al.*, 1995]. This may be explained by the great contrast in vegetation cover (deforested areas) that leads to convective motions and therefore shallow cumulus clouds. This is a permanent feature (during wet or dry season).

The boundary layer in wet season over tropical rain forest is not a source for ozone like in a polluted atmosphere but rather a sink [*Ritter et al.*, 1990; *Browell et al.*, 1990]. Between the boundary layer and the free troposphere, weak cumulus can take place and allow the vertical transfer of chemical species such as CO or O_3. These species play a important role in global tropospheric chemistry, and we must estimate the venting in all conditions (here there is shallow convection, above rain forest during the wet season).

In our study, the cloud transforms the fossil layer below 1500 m during the cloud development and "vents" a part of
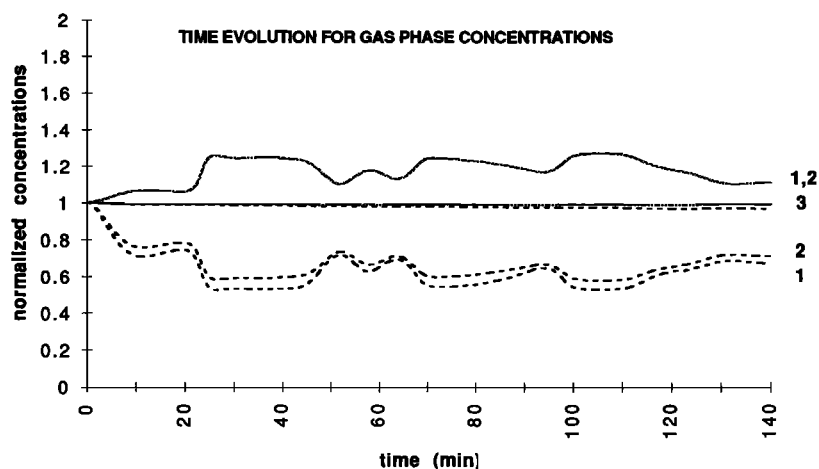

Figure 12. At 1500 m in center of convection, time evolution during 140 min of O_3 (dotted line) and CO (solid line) concentration normalized by initial value. Run 1: All the processes (dynamical, gas, and aqueous phases) are taken into account. Run 2: no transfer through the aqueous phase. Run 3: only gas chemistry.

content above 2000 m into the free troposphere. We evaluated during the whole simulation the CO and O_3 fluxes between the boundary layer at 1500 m and the free troposphere toward the cloud top. We have calculated the CO and O_3 net vertical fluxes between these levels. The CO and O_3 upward fluxes are respectively 7.7×10^{23} molecules km^{-2} h^{-1} and 1.2×10^{23} molecules km^{-2} h^{-1}. These amounts are about two hundred times smaller than those obtained for O_3 during deep convection (PRESTORM), with high value of NO, which are 7.97×10^{11} molecules cm^{-2} s^{-1}, that is 2.8×10^{25} molecules km^{-2} h^{-1} [Pickering et al., 1992; Thomson et al., 1994]. In addition, we see that the CO vertical transport is negligible versus O_3 transport.

6. Conclusions

We have presented a cloud convection model coupled with a chemical model describing the oxidation chains of CH_4 and CO in presence of NO_x in remote troposphere. A shallow cumulus cloud field has been simulated over tropical rain forest, during the wet season, with low values of O_3 and NO_x. The case under study represents a local system which includes an active mixing layer from surface to 1000 m capped by a fossil mixed layer between 1000 and 1500 m, cumulus clouds penetrate into this layer and exchanges between the different layers are examined. We have shown that when vertical motion is strong, the fossil mixed layer and the mixing layer are mixed so that the fossil layer is destroyed. By tracer analysis, we have shown exchanges exist between the lower layer (from surface to 500 m) and the free troposphere (above 2000 m) across the mixing and fossil layer. After the development of several cycles of cloud cells, when the cloud precipitates, we have two convection cells: the first one from the ground to 1000 m and the second one from 1300 to 2200 m where is found a cloud cell. At this time, the exchanges between the two layers are stopped.

The comparison between experimental and modeled CO and O_3 data are in good agreement. The cloud convection smoothes more the O_3 vertical profile than the CO one because CO is supplied from ground surface and is therefore more concentrated near the surface than in altitude, while the opposite occurs for O_3 which is destroyed very weakly within the atmosphere by photochemistry. Sensitivity tests show that the main process driving chemical species redistribution is the dynamical mechanism. The microphysical and chemical processes are of lower importance. We have shown that even small clouds perform transport or transformation in the boundary layer.

The O_3 and CO vertical fluxes between the boundary layer and the free troposphere through the cloud top, are respectively 1.2×10^{23} molecules $km^{-2} h^{-1}$ and 7.7×10^{23} molecules $km^{-2} h^{-1}$. In tropical region, over rain forest, with low O_3 levels, where several cumulus exist every day, the vertical fluxes of some chemical species (like O_3) cannot be neglected.

References

Browell, E. V., G. L. Gregory, R. C. Harriss, and V. W. J. H. Kirchhoff, Ozone and aerosol distribution over the Amazon basin during the wet season, J. Geophys. Res., 95, 16,887–16,902, 1990.

Cautenet, S., and B. Lefeivre, Contrasting behavior of gas and aerosol scavenging in convective rain: A numerical and experimental study in the African equatorial forest, J. Geophys. Res., 99, 13,013–13,024, 1994.

Chameides, W. L., and D. D. Davis, The free radical chemistry of cloud droplets and its impact upon the composition of rain, J. Geophys. Res., 87, 4863–4877, 1982.

Chatfield, R. B., and A. C. Delany, Convection links biomass burning to increased tropical ozone: However, models will tend to overpredict O_3, J. Geophys. Res., 95, 18,473–18,488, 1990.

Chaumerliac, N., R. Rosset, M. Renard, and E. C. Nickerson, The transport and redistribution of atmospheric gases in regions of frontal rain, J. Atmos. Chem., 14, 43–51, 1989.

Ching, J. K. S., and A. J. Alkezweeny, Tracer study of vertical exchange by cumulus clouds. J. Climatol. Appl. Meteorol., 25, 1702–1711, 1986.

Cutrim, E. M. C., D. W. Martin, and R. Rabin, Enhancement of cumulus clouds over highlands, savannah and deforestation lands in Amazonia, Ann. Geophys., 13, 309, 1995.

Fitzjarrald, D. R., K. E. Moore, O. M. R. Cabral, J. Scolar, A. O. Manzi, and L. D. de Abrau Sa, Daytime turbulent exchange between the Amazon forest and the atmosphere, J. Geophys. Res., 95, 16,825–16,838, 1990.

Garstang, M., et al., Trace gas exchanges and convective transports over the Amazonia rain forest, J. Geophys. Res., 93, 1528–1550, 1988.

Gidel, L. T., Cumulus cloud transport of transient tracers, J. Geophys. Res., 88, 6587–6599, 1983.

Graedel, T. E., and P. J. Crutzen, Atmospheric change. An Earth System Perspective, 446 pp., W. H. Freeman, New York, 1993.

Greco, S. R., M. Swap, M. Garstang, S. Ulanski, M. Shipham, R. C. Harris, R. Talbot, M. O. Andreae, and P. Artaxo, Rainfall and surface kinematic conditions over central Amazonia during ABLE 2B, J. Geophys. Res., 95, 17,001–17,014, 1990.

Greco, S., J. Scala, J. Halverson, H. L. Massie, W. K. Tao, and M. Garstang, Amazon coastal sqall lines, II, Heat and moisture transports, Mon. Weather Rev., 122, 623–635, 1994.

Grégoire, P. J., N. Chaumerliac, and E. C. Nickerson, Impact of cloud dynamics on tropospheric chemistry: Advances in modeling the interactions between microphysical and chemical processes, J. Atmos. Chem., 18, 247–266, 1994.

Harriss, R. C., G. W. Sachse, G. F. Hill, L. O. Wade, and G. L. Gregory, Carbon monoxide over the Amazon basin during the wet season, J. Geophys. Res., 95, 16,927–16,931, 1990.

Hesstvedt, E., O. Hov, and I. S. A. Isaksen, Quasi-steady-state approximations in air pollution modeling: Comparison of two numerical schemes for oxidant prediction, Int. J. Chem. Kinetics, 10, 971–994, 1978.

Houze, R. A., Observed structure of mesoscala convective systems and implications for large-scale heating, Q. J. R. Meteorol. Soc., 487, 425–461, 1989.

Jacob, D. J., Chemistry of OH in remote clouds and its role in the production of formic acid and peroxymonosulfate, J. Geophys. Res., 91, 9807–9826, 1986.

Jacob, D. J., and S. C. Wofsy, Budgets of reactive nitrogen, hydrocarbons, and ozone over the Amazon forest during the wet season, J. Geophys. Res., 95, 16,737–16,754, 1990.

Kessler, E., On the redistribution and continuity of water substance in atmospheric circulation, Meteorol. Monogr., 10(32), 84 pp., 1969.

Lafore, J. P., and M. W. Moncrieff, A numerical investigation of the organisation and interaction of the convective and stratiform regions of tropical squall lines, J. Atmos. Sci., 46, 521–544, 1989.

Lelieveld, J., and P. J. Crutzen, Influences of cloud photochemical processes on tropospheric ozone, Nature, 343, 227–233, 1990.

Lelieveld, J., and P. J. Crutzen, The role of clouds in tropospheric photochemistry. J. Atmos. Chem., 12, 229–267, 1991.

Lyons, W. A., R. H. Calby, and C. S. Keen, The impact of mesoscale convective systems on regional visibility and oxidant distribution during persistent elevated pollution episodes, J. Climatol. Appl. Meteorol., 25, 1518–1531, 1986.

Madronich, S., Photodissociation in the atmosphere, 1, Actinic flux and the effect of ground reflections and clouds, J. Geophys. Res., 92, 9740–9752, 1987.

Marshall, J. S., and W. M. Palmer, The distribution of raindrops with size, *J. Meteorol.*, 5, 165–166, 1948.

Martin, C. L., D. Fitzjarrald, M. Garstang, A. P. Oliveira, S. Greco, and E. Browell, Structure and growth of the mixing layer over the Amazonian rain forest, *J. Geophys. Res.*, 93, 1361–1375, 1988.

Pickering, K. E., A. M. Thompson, R. R. Dickerson, W. T. Luke, D. P. McNamara, J. P. Greenberg, and P. R. Zimmerman: Model calculations of tropospheric ozone production potential following observed convective events, *J. Geophys. Res.*, 95, 14,049–14,062, 1990.

Pickering, K. E., A. M. Thompson, J. R. Scala, W. K. Tao, J. Simpson, and M. Garstang, Photochemical ozone production in tropical squall line convection during NASA Global Tropospheric Experiment/ Amazon Boundary Layer Experiment 2A, *J. Geophys. Res.*, 96, 3099–3114, 1991.

Pickering, K. E., A. M. Thompson, J. R. Scala, W. K. Tao, R. R. Dickerson, and J. Simpson, Free tropospheric ozone production following entrainment of urban plumes into deep convection, *J. Geophys. Res.*, 97, 17,985–18,000, 1992.

Preiss, M., R. Maser, H. Franke, W. Jaescke, and J. Graf, Distribution of trace substances inside and outside of clouds, *Beitr. Phys. Atmos.*, 67, 341–351, 1994.

Renard, M., N. Chaumerliac, S. Cautenet, and E. C. Nickerson, Tracer redistribution by clouds in West Africa: Numerical modeling for dry and wet seasons, *J. Geophys. Res.*, 99, 12,873–12,883, 1994.

Ritter, A. J., D. H. Lenschow, J. D. W. Barrick, G. L. Gregory, G. W. Sachse, G. F. Hill, and M. A. Woerner, Airborne flux measurements and budget estmates of traces species over the Amazonian basin during the GTE/ABLE2B Expedition, *J. Geophys. Res.*, 95, 16,875–16,886, 1990.

Scala, J. R., Cloud draft structure and trace gas transport, *J. Geophys. Res.*, 95, 17,015–17,030, 1990.

Singh, H. B., D. Herlth, D. O'Hara, L. Salas, A. L. Torres, G. L. Gregory, G. W. Sachse, and J. F. Kasting, Atmospheric peroxyacetyl nitrate measurements over the Brasilian Amazon basin during the wet season: Relationships with nitrogen oxides and ozone, *J. Geophys. Res.*, 95, 16,945–16,954, 1990.

Stockwell, W. R., Communication to the Editor regarding "Lelieveld, J., and P. J. Crutzen, 1991: The role of clouds in tropospheric photochemistry, *J. Atmos. Chem.*, 12, 229–267, 1994.

Talbot, R. W., M. O. Andreae, H. Berresheim, D. J. Jacob, and K. M. Beeker, Sources and sinks of formic, acetic and pyruvic acids over central Amazonia, 2, Wet season, *J. Geophys. Res.*, 95, 16,799–16,811, 1990.

Thompson, A. N., K. E. Pickering, R. R. Dickerson, W. G. Ellis Jr., D. J. Jacob, J. R. Scala, W-K Tao, D. P. McNamara, and J. Simpson, Convective transport over the central United States and its role in regional CO and ozone budgets, *J. Geophys. Res.*, 99, 18,703–18,711, 1994.

P. Brémaud, Laboratoire de Physique Atmosphere, Université de l'ile de la Reunion, St. Denis, 95 France.

S. Cautenet and J. Edy, Laboratoire de Meteorologie Physique, Universite Blaise Pascal/CNRS, 24 Avenue des Landais, 63177 Aubière, France.